

Elastic Self-Healing during Shear Accommodation in Crystalline Nanotube Ropes

Haiyi Liang^{1,2} and Moneesh Upmanyu^{2,*}

¹*Department of Modern Mechanics, University of Science and Technology of China, Hefei, People's Republic of China*

²*Group for Simulation and Theory of Atomic-Scale Material Phenomena (stAMP), Materials Science Program, Division of Engineering, Colorado School of Mines, Golden, Colorado 80401, USA*

(Received 24 September 2004; published 15 February 2005)

Rigid-tube computations of simple (transverse) shear in crystalline nanotube ropes (CNTRs) reveal that shear modulus and strength increase and decrease with the tube radius, respectively. High modulus to strength ratios suggest that dislocations play a minor role during their plasticity. The computed shear moduli are in agreement with previous studies, although shape change and rolling-based shear may modify low strain and temperature behavior. The instability past the shear strength is due to shear localization via interlayer sliding, wherein stress relief results in significant elastic energy dissipation. Large-tube radius CNTRs accommodate large strains at minimal energetic cost during sliding, due to the increasingly cohesive and short range nature of the intertube potential. Fascinatingly, the crystal aids its recovery, implying that CNTRs may be promising materials for energy absorption and tribology.

DOI: 10.1103/PhysRevLett.94.065502

PACS numbers: 62.25.+g, 62.20.Dc, 62.20.Fe, 81.07.De

Nanotube bundles are rapidly emerging as one of the building blocks for practical nanoscale materials. In particular, crystalline nanotube ropes (CNTRs) consisting of identical, aligned single-walled nanotubes have been successfully grown via both self-assembly and guided assembly [1]. CNTRs exhibit superior, yet highly anisotropic physical and transport properties including thermoelectric power generation [2], hydrogen adsorption [3], field emission [4], and even superconductivity [5]. Experimental and computational studies have shown that CNTRs are perhaps one of the most anisotropic materials available. For example, in the small tube radius limit ($r_t < 25 \text{ \AA}$) where the internanotube interactions exert a decisive influence on the mechanical properties, the longitudinal elastic modulus of these ropes E_{zz} ($\sim 1 \text{ TPa}$) is an order of magnitude greater than the transverse bulk modulus, K_{xy} ($\sim 40 \text{ GPa}$) [6–9].

CNTRs can also absorb a large amount of elastic strain, yet they are susceptible to (axial and transverse) shear. Flexure experiments indicate shear moduli $c_{44} \sim 1 \text{ GPa}$ [7]. Prior atomistic-continuum computational studies have yielded transverse shear moduli G_{xy} in the range 1–20 GPa [10,11]. Here, we focus on elastic and plastic shear accommodation mechanisms in carbon CNTRs. We self-consistently extract the theoretical shear strength and the shear modulus of these materials. This enables us to resolve the current discrepancies in computed values in G_{xy} [10,11] and also extract the ratio of the shear strength to the modulus, thereby determining the extent of dislocation-based crystal plasticity during deformation of CNTRs.

We use a molecular (tubular) statics approach to simulate simple (transverse) shear of achiral (armchair) (n, n)-crystalline nanotube ropes. Shear response is studied well past the elastic limit. The quasi-2D calculations are performed in the rigid-tube limit, since (a) assembly of CNTRs has been mostly limited to $r_t < 25 \text{ \AA}$ [12], and (b) intratube (valence) forces are insignificant for these

tube radii following excellent agreement between rigid-tube and fully atomistic calculations of the bulk modulus [6,9].

Based on the 6–12 Lennard-Jones (LJ) description of van der Waals force between graphene surface elements, the axially averaged *intertube* potential can be shown to be [9]

$$U_{it}(R_{it}, r_t) = \frac{3\pi\rho}{8r_t^3} \left(-AI_1 + \frac{21BI_2}{32r_t^6} \right), \quad (1)$$

where R_{it} is the distance between tube centers and $\rho (= 4/3\sqrt{3}a_{C-C}^2)$ is the atomic surface density. $A (= 15.2 \text{ eV \AA}^6)$ and $B (= 24\,100 \text{ eV \AA}^{12})$ are the LJ parameters, and I_1 and I_2 are surface integrals dependent on the reduced intertube distance $R'_{it} = R_{it}/r_t$ [9]. Note that this intertube interaction is short ranged and negligible for $R_{it} \geq \sqrt{3}r_t$; i.e., it is limited to first nearest neighbors. The intertube potential reproduces well-known CNTR parameters such as equilibrium intertube spacing (R_{it}^{eq}), cohesive energy per atom U_c^{eq} , bulk modulus, etc.

Figures 1(a)–1(c) show the computational cell configurations during shear of a (16, 16) CNTR. The same geome-

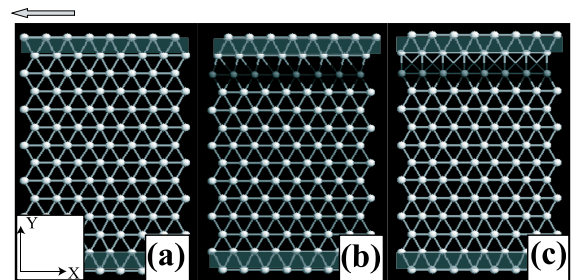


FIG. 1 (color online). Plots showing the transverse shear of the quasi-2D, (16, 16) CNTR, for (a) $\gamma_{xy} = 0.0\%$, (b) 2.7%, and (c) 5.8%. The block arrow is the direction of shear strain. Shaded strips indicate frozen (bottom) and displaced (top) atomic layers.

try with an identical number of tubes is used in all simulations. The fully periodic cell consists of 112 rigid tubes packed into a hexagonal lattice and divided into 14 rows, with 8 tubes per row. The conjugate gradient (CG) method is used to minimize the total system (interaction) energy. Equilibrated system energies U^{eq} and R_{it}^{eq} are in excellent agreement with atomistic calculations [6,9] and experiments (see Table I). The unstressed crystal is then subject to a shear strain in the transverse plane by (a) removing periodicity along the Y direction, (b) freezing the bottom two layers, and (c) prescribing displacements to the top two layers along the negative X direction. The static nature of the simulations allows control over the applied shear strain while avoiding high strain rates. Displacements of the top two layers are prescribed in steps of $0.1 R_{it}^{\text{eq}}$. After each step, CG-based relaxation of the entire tube system is performed along the Y direction, and system interaction energy $U(\gamma_{xy})$ and virial shear stress τ_{xy} are extracted. The virial stress is calculated for unconstrained tubes,

$$\tau_{xy} = -\frac{1}{2\Omega} \sum_i \sum_{j \neq i} f_{ij}^x r_{ij}^y \quad (2)$$

where Ω is the volume (area in 2D) per tube, f_{ij}^x is the force along the X direction on tube i due to tube j , and r_{ij}^y is the Y component of the vector distance between the two tubes [13]. The simulations are performed for $(4n, 4n)$ CNTRs, with $1 \leq n \leq 7$. The corresponding tube radii are in the range $2.7 \leq r \leq 19 \text{ \AA}$, well below the transition tube radii above which tube shape changes become important.

The complete shear response of the (16, 16) CNTR is shown in Figs. 1(a)–1(c). The top (displaced) and the bottom (frozen) two layers are shaded gray. The value of the shear strain γ_{xy} is also indicated. The shear strain dependence of the (excess) system elastic energy, $\Delta U = U(\gamma_{xy}) - U^{\text{eq}}$, and virial shear stress τ_{xy} are plotted in Fig. 2. The corresponding tube plots are also indicated in Figs. 1(b) and 1(c). As expected, the initial response for $\gamma_{xy} < 1\%$ is Hookean; the elastic energy and the shear stress vary parabolically and linearly, respectively, with the shear strain. The entire CNTR shears uniformly. The

slope of the stress-strain curve, the shear modulus is $G_{xy} = 25.6 \text{ GPa}$.

The nonlinear elastic response at higher strains is characterized by a decreasing shear modulus. At a critical point corresponding to the atomic plot Fig. 1(b) ($\tau_{xy}^* \approx 0.4 \text{ GPa}$, $\gamma_{xy}^* \approx 2.54\%$), the CNTR undergoes a substantial ($\sim 45\%$) and abrupt decrease in strain energy. Interestingly, the CNTR becomes almost stress-free. Figure 1(b) clearly shows that relaxation occurs due to shear localization via interlayer sliding at the top two layers. Then, τ_{xy}^* is the theoretical shear strength of the CNTR. The remaining crystal quickly recovers the shear stress, and the excess deformation energy is entirely due to interlayer sliding. Additional strain enhances sliding, *with little or no energetic cost and negligible shear stress*. The slip layers undergo a hexad-tetrad symmetry transition ($6mm \rightarrow 4mm$), as seen in Fig. 1(c). Further strain results in the recovery of the undeformed crystal; slip layers undergo a tetrad-hexad transition ($\gamma_{xy} > 10\%$). The deformation energy smoothly decreases, and shear is no longer localized. The nonlinear response gives way to Hookean elasticity ($\gamma_{xy} > 11\%$), with the shear modulus (slope) identical to that in the small strain regime ($\gamma_{xy} < 1\%$). Notice that the crystal develops a negative (clockwise) shear stress during this recovery period and recovers a significant fraction of the stored deformation energy (negative stress-strain area), leading us to conclude that the crystal *elastically self-heals*.

Figure 2 also shows the shear strain dependence of ΔU and τ_{xy} for (4, 4) and (28, 28) CNTRs. The behavior during the initial deformation and the final recovery, while quite similar, is sensitive to the tube radius. The shear modulus G_{xy} increases, while the shear strength τ_{xy}^* and the critical strain γ_{xy}^* decrease with increasing radius (see Table I). Perhaps of more interest is the interlayer sliding behavior, and the extent of *elastic self-healing*. The shear strain interval over which the interlayer sliding persists increases with increasing tube radius. For (4, 4) CNTRs, there is negligible sliding and the crystal undergoes a direct transition from uniform, nonlinear elastic deformation to recovery of the elastic energy. Thus, the tetrad interlayer structure is unstable with respect to incremental strain.

TABLE I. Extracted values of the equilibrium cohesive energy U_c^{eq} (meV/atom), the shear modulus G_{xy} (GPa), the critical shear strain γ_{xy}^* (%), the theoretical shear strength τ_{xy}^* (GPa), and the ratio $\xi = (\tau_{xy}^*/G_{xy})^{-1}$, as a function of tube radius r_t (\AA) in (n, n) CNTRs.

CNTR	r_t	$-U_c^{\text{eq}}$	G_{xy}	γ_{xy}^*	τ_{xy}^*	ξ
(4, 4)	2.7	27.5	13.2	7.0	0.6	22.8
(8, 8)	5.4	19.5	18.2	4.7	0.5	35.8
(12, 12)	8.1	16.0	22.2	3.4	0.5	49.4
(16, 16)	10.9	13.9	25.6	2.5	0.4	63.7
(20, 20)	13.6	12.5	28.6	2.0	0.4	77.7
(24, 24)	16.3	11.4	31.2	1.6	0.3	91.9
(28, 28)	19.0	10.6	33.7	1.4	0.3	105.8

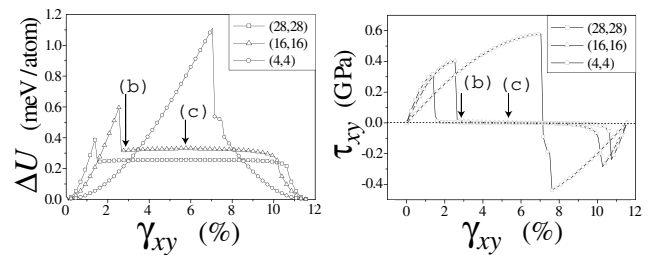


FIG. 2. Variation of the excess elastic energy ΔU (left) and the virial shear stress τ_{xy} (right) with the applied shear strain for three CNTRs. The arrows indicate the corresponding atomic plots in Fig. 1, for a (16, 16) CNTR.

Finally, the extent of elastic self-healing is proportional to the deformation energy stored in the CNTR, before the onset of shear localization; i.e., it decreases with an increasing tube radius.

In order to understand the radius dependence of G_{xy} , τ_{xy}^* , and γ_{xy}^* , it is instructive to analyze the tube radius dependence of the intertube potential, U_{tt} [Eq. (1)]. The depth of the potential well U_{tt}^{eq} (U_{tt} at $R_{tt} = R_{tt}^{\text{eq}}$) decreases with decreasing tube radius (see Table I). This trend can be seen in Fig. 3, a plot of the intertube potential as a function of the reduced intertube distance, R'_{tt} . However, the reduced equilibrium distance also decreases with an increasing tube radius. That is, the minimum pairwise distance between the nanotube surfaces (circumferential distance $R_{tt} - 2r_t$) is almost independent of the tube radius. Then, at equilibrium, the average interaction between the graphene surface elements on two different tubes is less attractive at larger tube radii, and the cohesive energy of the CNTR decreases. Atomistic calculations in the small radii limit also exhibited this trend; the cohesive energy varied as $U_c^{\text{eq}} \propto 1/\sqrt{r_t}$ [6]. Figure 3 also reveals that the attractive component of U_{tt}^{eq} is quite sensitive to the tube radius, more so than the repulsive part; the attractive tail rapidly decreases with increasing tube radius. Hence, at equilibrium, bulk modulus K_{xy} ($\propto d^2 U_{tt}/dR_{tt}^2$) increases with tube radius. This dependence on the tube radius should also translate to the shear modulus G_{xy} , where the reduced cohesive energy and the attractive tail render large-radii CNTRs increasingly susceptible to shear.

The effect of the tube radius on U_c^{eq} and the attractive tail of U_{tt} explains almost all other simulation trends (see Table I). The critical strain γ_{xy}^* for the onset of shear localization and the corresponding strength τ_{xy}^* again depend on system cohesive energy and vary accordingly. Strain interval associated with interlayer sliding depends

on the energetic cost of tetrad-hexad transition at the interlayer structure. The transition energy depends on the form of U_{tt} for $R_{tt} > R_{tt}^{\text{eq}}$; it decreases at a larger tube radius. This explains the enhanced strain accommodation via sliding at a larger tube radius. At a small tube radius, as in (4, 4) CNTR, there is little or no shear localization. The entire CNTR deforms uniformly into a tetrad interlayer structure, at which localization followed by deformation energy release occurs ($> 60\%$). The localization is unstable with respect to the additional strain, triggering shear recovery. The behavior follows from the longer attractive tail of the intertube potential. Further recovery proceeds with a substantial negative shear stress; i.e., the CNTR aids applied shear strain and self-heals elastically.

The elastic self-healing is fascinating, more so from the viewpoint of typical attractive-repulsive systems. The attractive component in LJ-based systems is sufficiently long range and cohesive, with a cutoff distance $R_{tt}^c \sim 2R_{tt}$ (inset of Fig. 3). The external force always does work against the system in order to shear it. To confirm, we repeated the simulations for CNTRs with equivalent LJ intertube potentials. At any stage, it is prohibitive to localize the shear at the expense of recovery of a significant portion, if not the entire CNTR, and $\tau_{xy} > 0$. The interlayer sliding is distributed over the layers, and the energetic cost is significant. Thus, we believe that shear localization and elastic self-healing are largely due to increasingly steric intertube interactions (square-well or hard sphere potential systems) at large-tube radii (Fig. 3).

Hybrid atomistic-continuum methods have been employed in the past to extract elastic constants of CNTRs, including G_{xy} [10,11,14]. Using an LJ-based rigid-tube approximation, Saether *et al.* [11] performed *pure shear* of a (12, 0) CNTR and showed that the shear modulus $G_{xy} = 22.5$ GPa. This value is in excellent agreement with our results for comparable tube radii, i.e. $G_{xy} = 25.6$ GPa for (16, 16) CNTRs. However, values from past pure shear studies using (radially) flexible tubes, with $r_t = 14.9$ Å and (a) axially averaged intratube interactions [10] as well as (b) hollow-shell approximation [15,16], are significantly smaller: 5.3 and 2.14 GPa, respectively. There, circular-elliptic shape transformations of individual tubes absorbed as much as 1% of the strain [16], with negligible tube translations. Evidently, the extracted shear modulus is due to the shape changes of individual tubes. Since the elastic energy to bend a (graphite) sheet goes as a square of the curvature, there is a finite limit to tube shape-change based strain accommodation. We expect a transition to translation-based shear, with a shear modulus close to the value extracted in this study. Slight deviations are expected due to the shape recovery during tube translations, thereby lowering τ_{xy}^* and γ_{xy}^* .

Practical considerations.—The ratio of the shear modulus to the theoretical shear strength $\xi = G_{xy}/\tau_{xy}^*$ is an indicator of the effect of dislocation-based crystal plasticity. For typical crystalline materials, $\xi \leq 30$. The tube

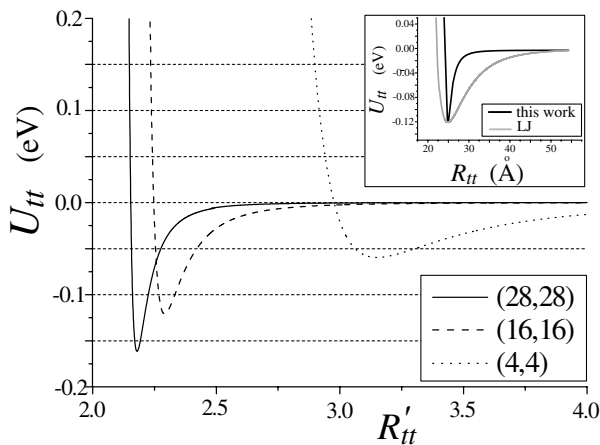


FIG. 3. Plot of the intertube potential U_{tt} versus the reduced intertube distance R'_{tt} , for (4, 4), (16, 16), and (28, 28) CNTRs. The inset shows the comparison between U_{tt} as per Eq. (1) and an equivalent (same minimum, equilibrium distance) LJ intertube potential.

radius dependence of ξ is tabulated in the last column in Table I. ξ increases with increasing tube radius, and the values lie in the range $22.83 < \xi < 105.8$. It can then be inferred that dislocation-based plasticity has little effect on the threshold (flow) stresses in large-tube radius CNTRs, and plays a minor role in their deformation behavior. Tube chirality will modify the shear deformation behavior. Chirality introduces anisotropic, orientation dependent intertube interactions. Below the orientational melting temperature T_m^ϕ , the tubes order into two-tube unit cells with well-defined relative orientations [17]. The orientational order is periodic. In (n, n) achiral nanotubes, the periodicity is $2\pi/n$. Clearly, the orientational order is disturbed during translation-based shear deformation. At a large radius, enhanced periodicity implies that roll-based shear can also take place. Then, shear deformation (including interlayer sliding) can be due to a combination of shape change, relative translation, and orientation change, or *roll*. These responses can also be coupled. As an example, at small tube radii, the large thermal dissipation past the shear strength can melt the orientational or structural order. Above T_m^ϕ , the orientational disorder is due to random diffusion of twistons along each nanotube. The shear behavior is even more complicated; possibly, localized rolling-based shear is quickly propagated over the entire length of the tubes via commensurate twistons (kink-antikink pairs). The entire CNTR develops long range orientational order. Thus, the initial shear deformation may be *entropic*, eventually leading into tube shape change and tube translation-based shear. In each of these regimes, we expect the shear modulus to be different. Fully atomistic calculations are currently being performed to study such behavior in greater detail [18].

In conclusion, we show that the shear accommodation in rigid-tube CNTRs ($r_t < 20 \text{ \AA}$) is sensitive to the tube radius. Linear elastic regime and shear strength increases, while shear modulus G_{xy} decreases with the tube radius. Extracted values of G_{xy} are in agreement with previous rigid-tube calculations. However, they are an order of magnitude larger compared to flexible-tube calculations, where the modulus is entirely due to tube shape changes. We also expect rolling-based shear to further modify the shear modulus, especially in large-tube radius, orientationally ordered CNTRs. The nonlinear elastic regime is characterized by a decreasing shear modulus as we approach the theoretical shear strength of the material τ_{xy}^* . The comparison of shear modulus and strength suggests that dislocation-based plasticity plays a minor role in the deformation behavior of large-tube radius CNTRs. Significant elastic recovery associated with subsequent localization via interlayer sliding implies that induced

adiabatic heating is significant, especially in low tube radius-based CNTRs. The large thermal dissipation can possibly result in local orientational and/or structural melting. Owing to the increasingly short range yet cohesive intertube potential at large-tube radii, we observe large strain accommodation via interlayer sliding. As the entire crystal recovers, it aids the shear recovery and *elastically self-heals*. Most of the deformation energy is recovered and the effect is more pronounced at low tube radii. The elastic self-healing response implies that CNTRs hold promise as lightweight, anisotropic, nanoscale materials for (shear) energy absorption, and as self-lubricating coatings in nanoscale tribological applications.

M. U. is grateful to Dr. V. Jindal and staff at Center for Advanced Physics, Panjab University, India, for their hospitality during the course of this study.

*Electronic address: mupmanyu@mines.edu

- [1] R. Dagani, Chem. Eng. News **74**, 5 (1996).
- [2] J. Hone, I. Ellwood, M. Munro, A. Mizel, M. L. Cohen, A. Zettl, A. G. Rinzler, and R. E. Smalley, Phys. Rev. Lett. **80**, 1042 (1998).
- [3] K. A. William and P. C. Eklund, Chem. Phys. Lett. **320**, 352 (2000).
- [4] N. S. Lee, D. S. Chung, and I. T. Han, Diam. Relat. Mater. **10**, 265 (2001).
- [5] J. Gonzalez, Phys. Rev. B **67**, 014528 (2003).
- [6] J. Tersoff and R. S. Ruoff, Phys. Rev. Lett. **73**, 676 (1994).
- [7] J. P. Salvetat, G. A. Briggs, J. M. Bonard, R. R. Bacsa, A. J. Kulik, T. Stockli, N. A. Burnham, and L. Forro, Phys. Rev. Lett. **82**, 944 (1999).
- [8] D. A. Walters, L. M. Ericson, M. J. Casavant, J. Liu, D. T. Colbert, K. A. Smith, and R. E. Smalley, Appl. Phys. Lett. **74**, 3803 (1999).
- [9] L. A. Girifalco, M. Hodak, and R. S. Lee, Phys. Rev. B **62**, 13 104 (2000).
- [10] V. N. Popov, V. E. van Doren, and M. Balkanski, Solid State Commun. **114**, 295 (2000).
- [11] E. Saether, S. J. V. Frankland, and R. B. Pipes, Compos. Sci. Technol. **63**, 1543 (2003).
- [12] J. Liu *et al.*, Science **280**, 1253 (1998).
- [13] The virial stress is in excellent agreement with the stress collected at the bottom frozen tube layers, and the second derivative of the energy density with respect to strain.
- [14] J. P. Lu, Phys. Rev. Lett. **79**, 1297 (1997).
- [15] B. I. Yakobson, C. J. Brabec, and J. Bernholc, Phys. Rev. Lett. **76**, 2511 (1996).
- [16] J. Z. Liu, Q.-S. Zheng, L.-F. Wang, and Q. Jiang, J. Mech. Phys. Solids **53**, 123 (2005).
- [17] Y. K. Kwon and D. Tománek, Phys. Rev. Lett. **84**, 1483 (2000).
- [18] H. Y. Liang and M. Upmanyu (to be published).